Articles

Investigating the Dynamic Properties of the Transmembrane Segment of Phospholamban Incorporated into Phospholipid Bilayers Utilizing ^{2}H and ^{15}N Solid-State NMR Spectroscopy†

Elvis K. Tiburu, Ethan S. Karp, Paresh C. Dave, Krishnan Damodaran, and Gary A. Lorigan*

Department of Chemistry and Biochemistry, Miami University, Oxford, Ohio 45056

Received May 4, 2004; Revised Manuscript Received August 20, 2004

ABSTRACT: ^{2}H and ^{15}N solid-state NMR spectroscopic techniques were used to investigate the membrane composition, orientation, and side-chain dynamics of the transmembrane segment of phospholamban (TM-PLB), a sarcoplasmic Ca^{2+}-regulator protein. ^{2}H NMR spectra of ^{2}H-labeled leucine (deuterated at one terminal methyl group) incorporated at different sites (CD_3-Leu28, CD_3-Leu39, and CD_3-Leu51) along the TM-PLB peptide exhibited line shapes characteristic of either methyl group reorientation about the $C_\gamma-C_\delta$ bond axis or by additional librational motion about the $C_\alpha-C_\beta$ and $C_\beta-C_\gamma$ bond axes. The ^{2}H NMR line shapes of all CD_3-labeled leucines are very similar below 0 °C, indicating that all of the residues are located inside the lipid bilayer. At higher temperatures, all three labeled leucine residues undergo rapid reorientation about the $C_\alpha-C_\beta$, $C_\beta-C_\gamma$, and $C_\gamma-C_\delta$ bond axes as indicated by ^{2}H line-shape simulations and reduced quadrupolar splittings. At all of the temperatures studied, the ^{2}H NMR spectra indicated that the Leu51 side chain has less motion than Leu39 or Leu28, which is attributed to its incorporation in the pentameric PLB leucine zipper motif. The ^{15}N powder spectra of Leu39 and Leu42 residues indicated no backbone motion, while Leu28 exhibited slight backbone motion. The chemical-shift anisotropy tensor values for ^{15}N-labeled Leu TM-PLB were $\sigma_{11} = 50.5$ ppm, $\sigma_{22} = 80.5$ ppm, and $\sigma_{33} = 229$ ppm within ±3 ppm experimental error. The ^{15}N chemical-shift value from the mechanically aligned spectrum of ^{15}N-labeled Leu39 PLB in DOPC/DOPE phospholipid bilayers was 220 ppm and is characteristic of a TM peptide that is nearly parallel with the bilayer normal.

Phospholamban (PLB)[1] is a homopentameric transmembrane (TM) protein that regulates Ca^{2+}-ATPase, which controls Ca^{2+} transport across the sarcoplasmic reticulum (SR), leading to muscle relaxation (*1*). Fuji and co-workers elucidated the complete primary structure of PLB by amino acid sequencing and found that the molecular mass of the PLB monomer is 6082 Da. Also, they determined that PLB is a pentamer consisting of five identical subunits (*2*). Mutagenesis studies of the TM domain section of PLB indicated that the monomeric form of PLB is a more effective inhibitor of Ca^{2+}-ATPase than the pentameric form (*3*, *4*). Thus, PLB inhibits SERCA2a, an isoform of Ca^{2+}-ATPase, in its unphosphorylated (monomeric PLB) form, whereas the phosphorylated (pentameric PLB) form dissociates from SERCA2a (*5*). Phosphorylation of PLB at Ser16 and Thr17 by both cAMP- and calcium/calmodulin-dependent protein kinases in response to β-adrenergic stimulation results in the formation of pentameric complexes (*6*). PLB is a 52 amino acid TM protein and consists of three structural domains: residues 1−20 that comprise the hydrophilic cytoplasmic domain, residues 21−30 that create a hinge segment, and residues 31−52 that encompass the hydrophobic α-helical membrane-spanning region (*7*, *8*). Solution NMR studies in organic solvents have shown that monomeric PLB has a disjointed structure, with the intervening domain as either a short flexible turn or a β-turn type-III conformation (*9*, *10*).

The α-helical TM segment of PLB consists of 22 amino acid residues (^{31}LFINFCLILICLLLICIIVMLL^{52}) and is believed to anchor the protein into the membrane (*11*, *12*). Engelman and co-workers utilized site-directed mutagenesis studies to define the interacting surfaces between the α

† This work was supported by the American Heart Association Scientist Development Grant (0130396N) and the NIH Grant (GM60259-01). The 500-MHz wide bore NMR spectrometer was obtained from NSF Grant (10116333).

* To whom correspondence should be addressed. E-mail: lorigag@muohio.edu. Fax: (513) 529-5715. Phone: (513) 529-3338.

[1] Abbreviations: CP-MAS, cross-polarization magic angle spinning; DMF, dimethylformamide; DIEA, *N*,*N*-diisopropylethylamine; DOPC, 1,2-dioleoylphosphocholine; EDTA, ethylenediaminetetraacetic acid; FA, formic acid; Fmoc, 9-fluorenyl-methoxycarbonyl; HBTU, *O*-benzotriazol-1-*N*,*N*,*N*,*N*-tetramethyluronium hexafluorophosphate; HEPES, *N*-[2-hydroxyethyl]piperizine-*N*-2-ethane sulfonic acid; HFIP, hexafluoro-2-propanol; HMP, 4-hydroxymethylphenoxymethyl copolystyrene-1% divinylbenzene resin; HOBT, 1-hydroxybenzotriazole; IPA, 2-propanol; L_α, liquid-crystalline phase; MALDI−TOF, matrix-assisted laser-desorption ionization time of flight; MeCN, acetonitrile; NMR, nuclear magnetic resonance; PLB, phospholamban; POPC, 1-palmitoyl-2-oleoyl-phosphocholine; SR, sarcoplasmic reticulum; TFA, trifluoroacetic acid; TFE, 2,2,2-trifluoroethanol; TM, transmembrane.

10.1021/bi0490993 CCC: $27.50
Published on Web 10/16/2004

helices of phospholamban that are responsible for the formation of the pentamer (*13*). Subsequent studies using chimeric constructs expressed in *Escherichia coli* explored a wide range of sequence alterations (*14*). SDS−PAGE assays were employed to determine the influence of substitution on pentamer formation (*14*). There is a repeating pattern of disruption when substitutions are made along the length of the PLB peptide, suggesting that the helices may interact with each other. Mutations at specific residues such as Leu37, Ile40, Leu44, and Leu47 disrupt pentamer formation and are thought to be involved in isoleucine/leucine zipper formations (*6*, *11*, *14*, *15*). The oligomeric state of phospholamban in lipid bilayers has also been determined using spin-labeled EPR and refined by molecular dynamic simulations. These studies suggest that these helical structures permit nonpolar side chains from one strand to fit into gaps in the surface of another strand, the "knobs-into-holes" bonding arrangement (*16*).

Furthermore, the inhibitory association of PLB with Ca^{2+}-ATPase involves both the cytoplasmic and TM domains of PLB (*17*−*19*). Phosphorylation of PLB activates the Ca^{2+} pump of the cardiac SR and increases the Ca^{2+} uptake by a mechanism that is still unclear (*20*). Thus, the dynamic regulation of the protein−protein interactions is the key to understanding the Ca^{2+} pump regulation by PLB. Direct measurement of protein dynamics and interactions using site-specific spectroscopic probes will be crucial to the elucidation of this molecular mechanism. Structural analysis through molecular dynamic techniques have been instrumental in understanding the motion and dynamics of PLB in the SR (*21*). The existence of a stable PLB pentamer in the SR and its small size makes it suitable for solid-state NMR spectroscopic studies.

There is still disagreement on the structure of PLB embedded in lipid membranes even though studies have shown that PLB readily associates in lipid bilayers to form a homopentamer, which has been shown to function as a Ca^{2+} channel (*22*, *23*). Presently, there are two structural models that have been proposed based upon spectroscopic studies and molecular-modeling techniques for pentameric PLB as shown in Figure 1 (*24*, *25*). In one model (Figure 1A), PLB is composed of two α helices connected by an unstructured/β-sheet region with the cytosolic domain tilted in a range of 50−60° with respect to the bilayer normal (*25*). Another model (Figure 1B) has proposed a continuous α helix of about 40 amino acid residues with a tilt angle of about 28° for PLB with respect to the bilayer normal (*24*).

Previous studies have shown that the TM helices alone are sufficient to drive pentamer formation thus, giving rise to interest in the residues that are involved in the structural organization of PLB (*6*, *26*).

Deuterium NMR spectroscopy is well-suited to study the structural and dynamic properties of membrane proteins in phospholipid bilayers (*27*−*30*). The technique has developed into an excellent probe for dynamic processes utilizing the corresponding quadrupolar splitting and line shapes (*31*, *32*). ^{2}H NMR spectroscopy has been used to study the molecular dynamics of side-chain residues in site-specific ^{2}H-labeled integral membrane proteins (*33*−*36*). The motions of the methyl groups in aliphatic side chains reflect those of the backbone and methylene sites of these residues. Selectively introducing a CD_3 group at a specific residue in a protein through peptide synthesis and to examine its corresponding quadrupolar splitting and line shape through NMR spectroscopy is a powerful technique used by many research groups (*15*, *34*, *37*). Methyl group motions have been well-characterized by ^{2}H NMR studies of CD_3-labeled sites of alanines and valines in other TM peptides (*38*−*41*). The primary amino acid sequence of the TM segment of PLB clearly shows a repeating pattern of isoleucine/leucine (isoleucine/leucine make up about 60% of the TM segment) residues along the length of the peptide. This suggests a possible interacting role of these residues in stabilizing the pentameric structure inside the membrane. Very limited information is available on ^{2}H solid-state NMR dynamic studies on long aliphatic side chains such as those of leucine for TM proteins such as PLB (*34*, *36*). This study will enhance our knowledge of long side-chain dynamics by investigating the motional properties of various CD_3 Leu residues of TM-PLB.

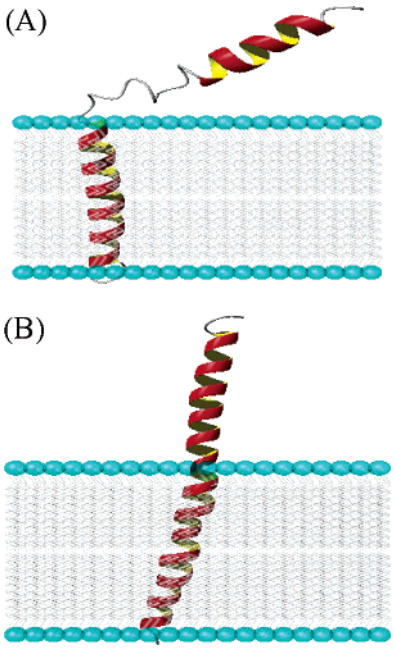

FIGURE 1: Two models representing the structure of monomeric PLB in phospholipid bilayers are depicted above. In model A, PLB has two α helices separated by an unstructured region presumed to be a β-sheet structure. In model B, PLB is a continuous α-helical protein.

For leucine residues, the side chain can be isotopically labeled at the δ- and/or ϵ-CD_3 sites and the deuterium NMR powder pattern line shapes will be strongly influenced by the motions about the $C_\gamma-C_\delta$ bond axis and by additional librational motion about the $C_\alpha-C_\beta$ and $C_\beta-C_\gamma$ bond axes at various temperatures (*34*, *42*). Furthermore, knowledge of the precise location of the residues within the bilayer is required for understanding the structural and dynamic organization of the peptide within the membrane.

For solid-state ^{2}H NMR spectroscopy, the allowed transitions correspond to $+1 \leftrightarrow 0$ and $0 \leftrightarrow -1$ and give rise to a quadrupolar splitting of the absorption line with separation $\Delta\nu$ between peak maxima (assuming an axial symmetric electric field gradient tensor) of

$$\Delta\nu = (3/4)(e^2qQ/h)(3\cos^2\theta - 1) \qquad (1)$$

where e^2qQ/h is the quadrupole coupling constant and θ

defines the orientation of the principal axis of the electric field gradient tensor with respect to the laboratory coordinate system (*35*). Generally, for CD_3-Leu in a polycrystalline solid, all values of θ are possible and the so-called "powder pattern" is obtained, having a quadrupolar splitting ($\Delta\upsilon$) of 127 kHz for solid aliphatic chains (*35*, *43*). Three-fold methyl hops or rotations cause a reduction in $\Delta\upsilon$ from 127 to 40 kHz (*44*). However, such spectra still retain an axially symmetric gradient tensor. Further reduction in the splitting followed by a certain degree of asymmetry in the spectra can be caused by additional motions such as (i) rotational motions about the peptide long molecular axis, (ii) rotation about the $C_\alpha-C_\beta$ and $C_\beta-C_\gamma$ bond axes, (iii) librational motions associated with wobbling of methyl groups, or (iv) backbone mobility (*44*, *45*).

In addition, selective $^{13}C-^{13}C$ and $^{13}C-^{15}N$ interatomic distances along the backbone of wild-type PLB have been measured via solid-state NMR spectroscopic techniques such as rotational-echo double resonance (REDOR) and rotational resonance (*23*). The results suggest that the wild-type PLB is pentameric with an α-helical structure. However, ^{15}N solid-state NMR studies involving the mutant analogue of the AFA-PLB (where A36, F41, and A46 have replaced the three corresponding TM cysteine residues) monomer in uniaxially aligned lipid bilayers have shown that the TM and cytosolic domains are perpendicular to each other (*8*). The conflicting results may reflect structural differences between the pentameric and monomeric forms of PLB because of conformational changes. Thus, it is one objective of this study to use site-specific isotopically labeled TM-PLB peptides to probe the backbone and side-chain motions of the TM segment of the wild-type PLB in phospholipid bilayers.

In the present study, several TM-PLB peptides were synthesized with selective incorporation of ^{15}N- or ^2H-labeled leucine at specific positions. We have examined side-chain motions of [5,5,5-$^2H_3$]Leu-labeled TM-PLB at residues Leu28, Leu39, and Leu51 separately incorporated into 1-palmitoyl-2-oleoyl-phosphocholine (POPC) bilayers to investigate the structural and dynamic properties of the leucine side chain using solid-state ^2H NMR spectroscopy. Also, ^{15}N-labeled TM-PLB at residues Leu28, Leu39, and Leu42 were studied using both ^{15}N static and ^{15}N CP-MAS NMR spectroscopy to investigate backbone mobility. Using the anisotropic ^{15}N chemical shift as an orientational constraint, single-site ^{15}N-labeled TM-PLB (at residue Leu39) was studied in 1,2-dioleoylphosphocholine (DOPC) bilayers oriented between thin glass plates. The resultant ^{15}N chemical shift provided helical orientational information for TM-PLB with respect to the membrane.

MATERIALS AND METHODS

Materials. Fmoc amino acids and other chemicals for peptide synthesis were purchased from Applied Biosystems Inc. (Forster City, CA). Fmoc-leucine-5,5,5-d_3 and Fmoc-leucine-^{15}N derivatives were purchased from Isotec Inc. (Miamisburg, OH). ^2H-depleted water was purchased from Isotec Inc. POPC and DOPC were purchased from Avanti Polar Lipids Inc. (Alabaster, AL). The phospholipids were shipped already dissolved in chloroform at a concentration of 20 mg/mL and stored at −20 °C. Chloroform, hexafluoro-2-propanol (HFIP), formic acid, and 2,2,2-trifluoroethanol (TFE) were purchased from Sigma−Aldrich Chemical Co. (St. Louis, MO). HPLC-grade acetonitrile and 2-propanol were obtained from Pharmco (Brockfield, CT) and were filtered through a 0.2-μm nylon membrane before use. Water was purified using a Nanopure reverse osmosis system (Millipore, Bedford, MA). *N*-[2-Hydroxyethyl]piperizine-*N*-2-ethane sulfonic acid (HEPES), trifluoro acetic acid (TFA), and ethylenediaminetetraacetic acid (EDTA) were also obtained from Sigma−Aldrich Chemical Co.

Peptide Synthesis. Several ^2H- and ^{15}N-labeled TM-PLB peptides were synthesized using predefined procedures (*46*). The polypeptides corresponding to TM-PLB, Ala24-Leu52 (^2H-Leu PLB and ^{15}N-Leu PLB) were synthesized on an Applied Biosystems Inc. (ABI) 433A solid-phase peptide synthesizer controlled by a G3 Macintosh computer with SynthAssist 2.0 software as described previously (*46*).

Peptide Purification. The synthesized ^2H- and ^{15}N-labeled TM-PLB peptides were purified using the following procedure. The synthesized peptide was removed from the synthesizer and cleaved from the resin. The lyophilized peptide was dissolved in HFIP/FA (4:1, at a concentration of 5 mg/mL) and centrifuged to eliminate insoluble particulates. The crude peptide was purified on an Amersham Pharmacia Biotech AKTA Explorer 10S HPLC controlled by Unicorn version 3 system software. A polymer-supported column (259 VHP82215, 5 μm, 300 Å pore size, 2.2 × 15 cm) from Grace-Vydacc was used to purify TM-PLB. The column was equilibrated with 95% solvent A/5% solvent B. Solvent A consisted of H_2O and 0.1% TFA and solvent B was 38% MeCN, 57% IPA, and 5% H_2O (*46*). A 1-mL aliquot of the (5 mg/mL) peptide sample was injected into the column, and the gradient was ramped from 5 to 100% of solvent B at a flow rate of 10 mL/min. Peptide elution was achieved with a linear gradient to a final solvent composition of 93% solvent B. The purified peptide fraction was lyophilized and analyzed by MALDI−TOF mass spectroscopy using a matrix of 2,5-dihydroxybenzoic acid. The overall yield of TM-PLB was about 37% (*46*).

Solid-State NMR Sample Preparation. For the ^2H NMR experiments, 76 mg of POPC dissolved in chloroform was mixed with 13.4 mg of appropriately ^2H-labeled TM-PLB (residues 24−52) (i.e., 4 mol % with respect to POPC) dissolved in a minimal amount of TFE. The sample was dried by passing a stream of nitrogen gas over the sample in the flask and then dried in a vacuum desiccator overnight. HEPES buffer (190 μL), prepared in ^2H-depleted water (5 mM EDTA, 20 mM NaCl, and 30 mM HEPES at pH 7.0), was added to the peptide/lipid mixture in a 12 × 75 mm test tube, and the peptide/lipid mixture was allowed to sit in a water bath at 50 °C for 30 min. The peptide/lipid mixture was occasionally agitated on a vortexer until a homogeneous phase was established. The sample was loaded into a flat-bottom round glass tube of 5 mm outside diameter for the NMR spectroscopy studies.

After the ^{15}N NMR powder sample was dried overnight in the desiccator, it was transferred and packed into a 4-mm ZrO_2 rotor. The hydrated sample was prepared by placing the rotor containing the dry sample in a relative humidity (~93%) chamber of saturated ammonium monophosphate. The sample was incubated for 6−12 h at a temperature of about 45 °C.

The mechanically aligned ^{15}N-labeled sample was prepared by cosolubilizing TM-PLB and DOPC/DOPE (4:1) in chloroform at a 1:200 mole ratio. The TM-PLB peptide was dissolved in a minimal amount of TFE prior to cosolubilizing with the lipids. The solution was spread onto 30 (8.5 × 14 mm) glass plates and allowed to air-dry for 30 min before vacuum drying for another 24 h. Deuterium-depleted water was added onto the peptide/lipid mixture, and the glass plates were stacked on top of each other. The stacked glass plates were then placed in a humidity chamber consisting of saturated ammonium monophosphate at a relative humidity of about 93% at 42 °C for 12 h.

^{2}H Solid-State NMR Spectroscopy. All ^{2}H solid-state NMR spectra were acquired on a Bruker Avance 500 MHz WB solid-state NMR spectrometer operating at a resonance frequency of 76.8 MHz for ^{2}H using a double-resonance solid-state NMR probe equipped with a 5-mm solenoid coil. The quadrupolar echo-pulse sequence was used with quadrature detection capabilities and complete phase cycling of the pulse pairs (*47*). A 3.0-μs 90° pulse, 100-kHz sweep width, 400-ms recycle delay time, and 30-μs interpulse delay were used to accumulate 150 000 transients. Prior to Fourier transformation, an exponential multiplication with 200-Hz line broadening was performed on the spectra. The spectra were acquired over a temperature range from −25 to 60 °C.

^{15}N Solid-State NMR Spectroscopy. Unoriented membrane protein samples were placed into a 4-mm sample rotor and inserted into a Bruker triple resonance CP-MAS solid-state NMR probe (Bruker Avance 500 MHz WB solid-state NMR spectrometer) operating at 50.7 MHz for ^{15}N. ^{15}N solid-state NMR spectra were collected utilizing a standard cross polarization pulse sequence with ^{1}H decoupling (*48*). The following pulse sequence parameters were used: 4.3-μs ^{1}H 90° pulse, 500-ppm sweep width, 1.5-ms contact time, and 4-s recycle delay with ^{1}H decoupling. Samples were spun at 5 kHz for the CP-MAS experiments. A total of 40-k scans were averaged for the static experiments, and 4-k scans were averaged for the CP-MAS experiments. The spectra were referenced to an external standard of $(^{15}NH_4)_2SO_4$ (27 ppm). The experiments were recorded at temperatures ranging from −25 to 25 °C.

The mechanically aligned ^{15}N spectrum was collected using a Bruker double-resonance flat-coil solid-state NMR probe operating at 25 °C. A standard cross-polarization pulse sequence was used with the following parameters: 4.5-μs ^{1}H 90° pulse, 1.0-ms contact time, 600-ppm sweep width, and a 4-s recycle delay with ^{1}H decoupling. A total of 24-k scans were averaged, and 300-Hz line broadening was used to process the data.

NMR Data Analysis. Simulations of the ^{15}N NMR spectra were carried out using the DMFIT software program that is capable of modeling one- and two-dimensional solid-state NMR spectra (*49*). The principal elements of the chemical-shift tensors are represented according to the convention $\sigma_{33} \geq \sigma_{22} \geq \sigma_{11}$.

Leucine deuterium line-shape simulations were performed using two independent axes defined with the MXQET software program (*50*). The first axis defined the tetrahedral three-site methyl group hopping in which the deuterons were tilted 75° with respect to the axis and with jumps of 120°. The second axis defined two-site methyl group jumping in which the methyl groups are tilted 75° and jump by 109.5°.

$$\overset{28}{\text{A}}\text{RQNL}\overset{39}{\text{Q}}\overset{42}{\text{N}}\text{LFINFCLILICLLLICIIVML}\overset{51}{\text{L}}$$

FIGURE 2: Amino acid sequence corresponding to part of the hinge region and the TM region of PLB is shown above. The amino acids in bold face represent the ^{2}H- or ^{15}N-labeled sites used in this study.

The asymmetry parameter (η) was 0.05 for all of the ^{2}H NMR simulations (*34*).

RESULTS

The sequence corresponding to the peptide representing TM-PLB is displayed in Figure 2. The sequence represents part of the hinge segment (residues 24−30) and the entire TM segment (residues 31−52) of PLB. The specific isotopically labeled sites (^{2}H- and ^{15}N-labeled) are indicated with numbers above them as shown below.

The placement of the site-specific isotopically labeled residues was based upon the following conditions; Leu28 was chosen to be toward the N terminus of the peptide and close to the cytosolic side of the membrane. Other residues were chosen so that they would be buried within the phospholipid bilayers (Leu39 and Leu42), and Leu51 was chosen because it is located toward the C terminus and either close to the headgroup of the phospholipid bilayer or buried within the phospholipid hydrophobic core.

^{2}H Side-Chain Dynamics. Figure 3 shows the solid-state ^{2}H NMR powder pattern spectra of specific labeled CD_3-Leu28, CD_3-Leu39, and CD_3-Leu51 TM-PLB samples incorporated into unoriented POPC bilayers. The spectra were recorded over the temperature range from −25 to 60 °C.

In the gel phase (−25 °C), the deuterium line shapes and quadrupolar splittings indicate that the only significant motion is methyl group rotation, because global motion is eliminated from the spectra by lowering the temperature of the sample below the gel−liquid-crystalline phase transition of −3 °C (*34*). The quadrupolar splittings, $\Delta\upsilon$, for all three leucines are slightly different. The CD_3-Leu28, CD_3-Leu39, and CD_3-Leu51 spectra revealed quadrupolar splittings of about 30, 32, and 36 kHz, respectively. The ^{2}H line shapes of Leu28 and Leu39 are broad and rounded (bell-like shape), whereas the spectrum corresponding to Leu51 has a flatter top powder line shape characteristic of more restricted motion. The marginal differences in the splitting and the line shapes for all three leucines is attributed to the slightly different environment of these residues within the bilayer.

At 0 °C, which is very close to the liquid-crystalline phase transition of the POPC phospholipids, additional leucine side-chain motions are involved that decrease the quadrupolar splitting of CD_3-Leu28 and CD_3-Leu39 significantly. The ^{2}H peak centered at 0 kHz in the three spectra is due to residual ^{2}H nuclei in the ^{2}H-depleted water. Upon heating the sample to 25 °C, there is a dramatic change in the spectral width of the CD_3-Leu28 spectrum characterized by a relatively narrow Pake doublet peak, which exhibits a ^{2}H line shape that is characteristic of a $\eta > 0$ pattern (*44*). This is explained by an increase in side-chain motions associated with 2-fold jumps between predominant leucine side-chain rotamers as well as 3-fold methyl group reorientations (*15*). This causes a reduction in the spectral width with a quadrupolar splitting of about 6 kHz, a typical value for leucine buried within the hydrophobic region of a membrane

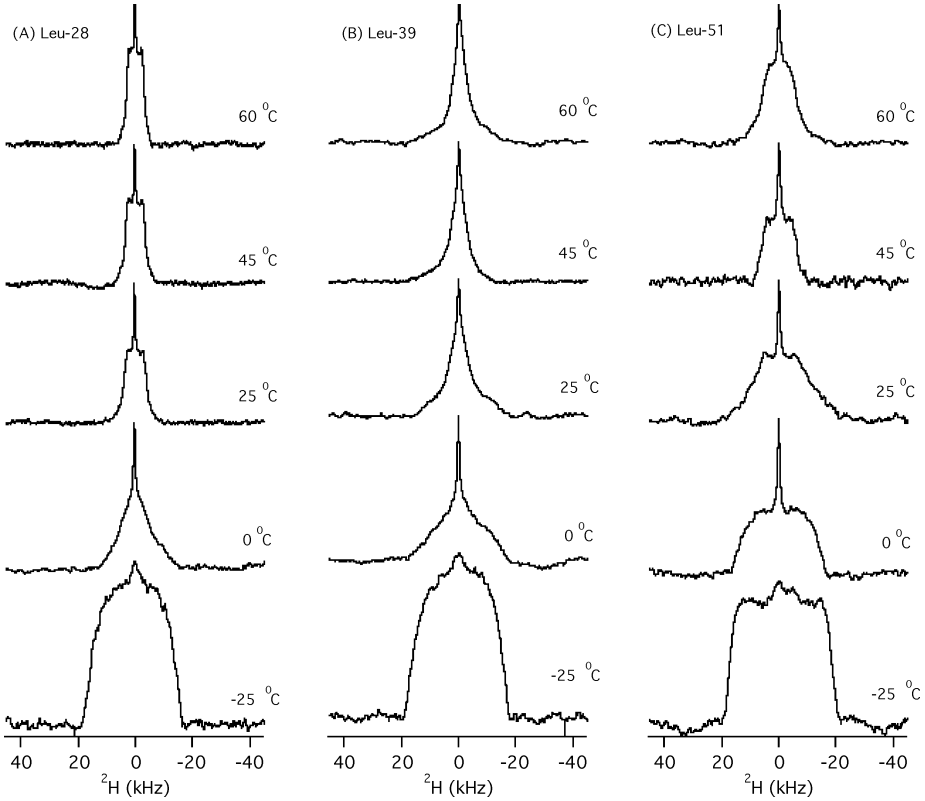

FIGURE 3: ^{2}H NMR powder pattern spectra of L-leucine-5,5,5-d_3 incorporated at specific sites of TM-PLB and inserted into POPC phospholipid bilayers. ^{2}H NMR spectra are shown for (A) CD_3-Leu28 PLB, (B) CD_3-Leu39 PLB, and (C) CD_3-Leu51 PLB incorporated into POPC phospholipid bilayers at lipid/peptide molar ratios of 25:1. The experiments were conducted at temperatures ranging from −25 to 60 °C. A total of 150 000 transients were accumulated for each spectrum and processed with a line broadening of 200 Hz.

at that temperature (*29*). Small changes in the quadrupolar splitting are observed at higher temperatures (45 and 60 °C), indicating faster motional averaging attributed to faster 2- and 3-fold jump rates. The shoulders at the edge of the powder are due to rapid methyl group reorientations that are faster than the NMR time scale (10^{-4} s). Our current model of TM-PLB suggests that Leu28 is located toward the N terminus of the peptide, which is often a more mobile section of a TM α helix (*38*).

At 25 °C, CD_3-Leu39 exhibits a spectral line shape with characteristics not typical of Pake doublets, and this may be due to additional modes of motions (*32*). The narrow Lorentzian line shapes are indicative of either fast side-chain reorientation both rapidly and isotropically or off-axis motion. At higher temperatures (45 and 60 °C), the spectral line shapes are maintained, although the breadth observed at 25 °C has eventually merged with the isotropic peak. The disappearance of the breadth component at higher temperatures could also be due to global motion of the peptide along the long molecular axis and increased librational motions of the side chain resulting in an averaging of the electric field gradient tensors and consequently giving a narrow powder pattern line shape (*45*).

At 25 °C, ^{2}H NMR powder spectra of CD_3-Leu51 exhibit bell-shaped characteristics indicative of slower methyl group reorientations than the NMR time scale. The appearance of a small Pake doublet at this temperature could also indicate the presence of a more rapidly moving population of PLB superimposed on a slower, broader component. Narrowing of the spectra is further observed at higher temperatures (45 and 60 °C) but not as significantly as in the CD_3-Leu28 and CD_3-Leu39 spectra. The unique features associated with these spectra could be explained by the condition that the Leu51 side chain is involved in the so-called "knobs-into-holes" bonding arrangement in which the side chain of Leu51 from one α helix is locked into the groove of a second α helix (of the pentamer); therefore, the two α helices are coiled around each other. Smith and co-workers have also reported that Leu44 is buried within the core of pentameric phospholamban and also observed the general bell-shaped characteristics (*34*). This type of structural arrangement is believed to help stabilize the structure of the pentamer (*6*, *11*, *15*).

^{15}N Backbone Dynamics. The ^{15}N chemical-shift powder pattern from unoriented PLB protein samples in lipid bilayers can distinguish between mobile and rigid backbone sites on the 10^{-4}-s time scale (*36*). Generally, it has been found that ^{15}N spectral line shapes of unoriented samples provide reliable evidence for the presence of mobile sites. To determine the degree of backbone mobility of TM-PLB in POPC bilayers, site-specific ^{15}N-Leu TM-PLB peptides were incorporated into POPC phospholipid bilayers and the spectra were collected at −25 and 25 °C. ^{15}N CP-MAS spectra were collected for each of the samples at a spinning speed of 5 kHz. Figure 4D shows the ^{15}N CP-MAS spectrum of Leu28. All spectra showed single isotropic peaks near 120 ppm. The ^{15}N static chemical-shift powder pattern spectra of the hydrated samples of ^{15}N-Leu TM-PLB (Leu28, Leu39, and Leu42) in POPC bilayers are displayed in Figure 4 at 25 °C. The smooth axially symmetric powder patterns (A−C)

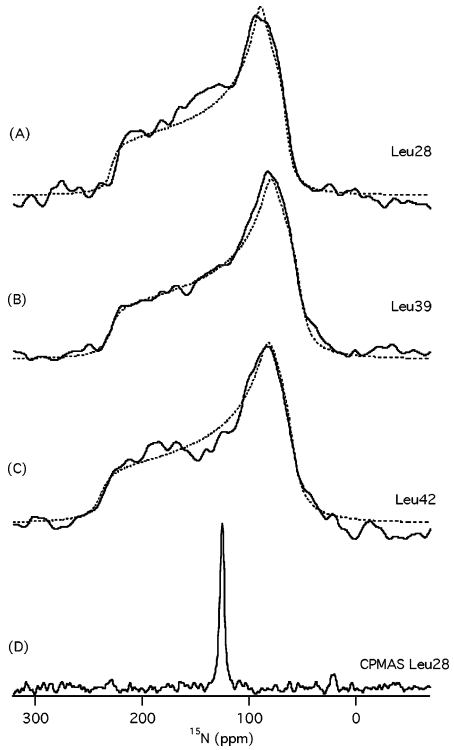

FIGURE 4: ^{15}N NMR powder pattern spectra of ^{15}N-labeled TM-PLB incorporated into POPC bilayers at a lipid/peptide ratio of 25:1. The static powder pattern spectra of (A) Leu28, (B) Leu39, and (C) Leu42 were obtained after 200 000 transients were collected. The experimental spectra were collected at 25 °C after hydration in a relative humidity chamber (93%) for 12 h. The simulated solid-state NMR spectra (···) are superimposed on the experimental spectra for comparison. Chemical-shift anisotropy values, with errors within ±3 ppm, were calculated from the simulated spectra and are shown in Table 1. (D) High-power proton-decoupled CP-MAS spectrum of hydrated ^{15}N-labeled Leu28 PLB inserted into POPC bilayers and spun at 5 kHz.

and the absence of any major isotropic components are an indication that the TM-PLB peptide has limited backbone mobility in the POPC phospholipid bilayers.

CP-MAS chemical-shift values of about 129 ppm are characteristic of β-sheet structures, whereas chemical-shift values lower than 122 ppm are characteristic of an α helix (*51*). The CPMAS chemical-shift value of 120 ppm corresponds to a leucine residue contained within an α-helical structure in a lipid bilayer, implying the parameters found in the powder pattern spectra are relevant to the secondary structure of TM-PLB in POPC phospholipid bilayers. The line shapes and intensities of the ^{15}N NMR spectra exhibited small deviations from each other at each labeled site along the backbone, indicating the absence of motional averaging and that the residues are all TM. Also, the line shapes for specific sites exhibited small changes as the temperature was increased from −25 °C (data not shown) to 25 °C.

Thus, the experimental spectra in Figure 4 show ^{15}N amide powder pattern spectra indicative of leucines in TM-PLB that have immobile peptide bonds located inside the membrane (*36*). This conclusion is further supported by the appearance of a single resonance peak and the absence of any other components in the CP-MAS spectra (one example is shown in Figure 4D). Thus, highly constrained backbone sites of TM-PLB suggest that the side-chain dynamics are not influenced by backbone fluctuations.

Table 1: ^{15}N Chemical-Shift Tensor Values of ^{15}N-Labeled TM-PLB (Leu28, Leu39, and Leu42) Inserted into POPC Phospholipid Bilayers[a]

	CSA values measured from single-site ^{15}N-labeled Leu-PLB powder samples [in ppm relative to $(^{15}NH_4)_2SO_4$ solution referenced to 27 ppm]				
sites	σ_{11}	σ_{22}	σ_{33}	σ_{iso}	CSA
Leu^{28}PLB	55.0	82.5	225.0	121.0	170.0
Leu^{39}PLB	50.5	80.5	229.0	120.0	178.0
Leu^{42}PLB	52.0	84.8	230.0	121.0	179.0

[a] These values were extracted from the simulated solid-state NMR spectra in Figure 3.

The experimental spectra of Figure 3 were simulated, and the results are displayed as dotted lines. The experimental spectra and the simulated spectra were superimposed, and the chemical-shift tensor elements were extracted from the single-site-labeled TM-PLB peptides. The chemical-shift tensor elements are displayed in Table 1 for comparison. The ^{15}N chemical-shift tensor values for ^{15}N-Leu39 PLB were found to be $\sigma_{11} = 50.5$, $\sigma_{22} = 80.5$, and $\sigma_{33} = 229 \pm 3$ ppm. These values are comparable to other ^{15}N tensoral components found in the literature (*51*). Similar parameters were also obtained from the ^{15}N-labeled Leu42 sample (Table 1). The observation of chemical-shift values close to the extremes of the chemical-shift anisotropy and the absence of any isotropic components demonstrates that all of the labeled residues investigated are TM and are motionally restricted by interactions with the lipid membrane (*52*).

However, it is interesting to note that the CSA corresponding to Leu28 was about 170 ppm, which is less than the CSA corresponding to Leu39 (178 ppm) and Leu42 (179 ppm). This implies that slight backbone motion is centered around Leu28 when compared to the other residues.

Helical Orientation of TM-PLB with Respect to the Lipid Bilayer Normal. The one-dimensional ^{15}N solid-state NMR spectrum of ^{15}N-labeled Leu39 PLB was obtained in fully hydrated DOPC/DOPE bilayers mechanically aligned on glass plates. As expected for a well-oriented sample, the spectrum in Figure 5A consists of a relatively narrow single line with a resonance frequency within the span of the ^{15}N chemical-shift anisotropy powder pattern.

An amide N−H bond approximately parallel to the direction of the static magnetic field and the membrane normal has an ^{15}N resonance frequency near that of the principal tensor element $\sigma_{\|}$. Conversely, an amide N−H bond perpendicular to the field and membrane normal has an ^{15}N resonance frequency near that of the principal tensor element $\sigma_{\perp}$ of the chemical-shift powder pattern spectra. A comparison of the spectra in Figure 5 clearly shows the effect of sample orientation. The most striking feature of the aligned spectrum shown in Figure 5A is that the single-line ^{15}N resonance observed from the specific ^{15}N-labeled Leu39 sample has a frequency near the $\sigma_{\|}$ edge of the amide chemical-shift powder pattern in Figure 5B. Thus, the chemical-shift value of 220 ppm indicates that the peptide plane is TM and nearly parallel with the membrane normal and the static magnetic field in aligned DOPC/DOPE phospholipid bilayers. This is further evidence that the PLB peptide has been successfully incorporated into DOPC/DOPE bilayers.

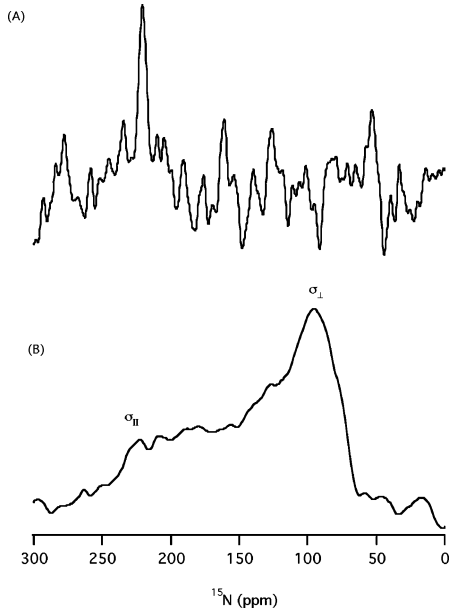

FIGURE 5: (A) One-dimensional solid-state ^{15}N NMR spectrum of ^{15}N-labeled Leu39 PLB inserted into DOPC/DOPE phospholipid bilayers mechanically oriented on glass plates. (B) For comparison, the solid-state ^{15}N NMR spectrum of ^{15}N-labeled Leu39 PLB inserted into unoriented POPC phospholipid bilayers. The ^{15}N NMR spectra were referenced to external $^{15}NH_4(SO_4)_2$ at 27 ppm.

DISCUSSION

Dynamics of TM-PLB in Phospholipid Bilayers. Model membranes have been used in recent years to study the orientation and dynamics of membrane-bound proteins in both randomly dispersed and oriented systems (*36*, *53*−*57*). Even though the study of such systems is challenging, especially when the lipids are in the liquid-crystalline phase characterized by a high degree of molecular disorder, much progress has been made in terms of understanding the physiological role and structure of integral-membrane proteins (*29*). The current study summarizes our understanding of the dynamics of side-chain leucines, the location, and the backbone mobility of TM-PLB in model membranes of POPC. The general shapes of the spectra are discussed in terms of pentameric TM-PLB incorporated into phospholipid bilayers. Several labs have shown that a PLB/lipid mole ratio as low as 1:100 will spontaneously assemble into a pentamer in DOPC phospholipid bilayers (*16*, *58*, *59*). However, such studies have also indicated the possibility of a dynamic exchange between monomeric and pentameric structures of full-length PLB (*16*, *58*, *59*).

Structural Implications of the Leucine Side-Chain Motions of TM-PLB in Lipid Bilayers. It is assumed in all of our discussions that the Leu side chain exists predominantly in only 2 of the 9 rotamer conformations separated by an angle of about 110° (*44*, *60*). Previous studies by Ying and co-workers *(34)* indicated that rotational, jumping, and librational motions about these bonds result in unique features of the deuterium line shapes. Wittebort and co-workers have used ^{2}H NMR spectroscopy to analyze line shapes in anisotropic media (*61*). To better understand the dynamics of our ^{2}H side-chain motion, the spectra shown in Figure 3 were simulated and representative best fits of the data are displayed in Figure 6.

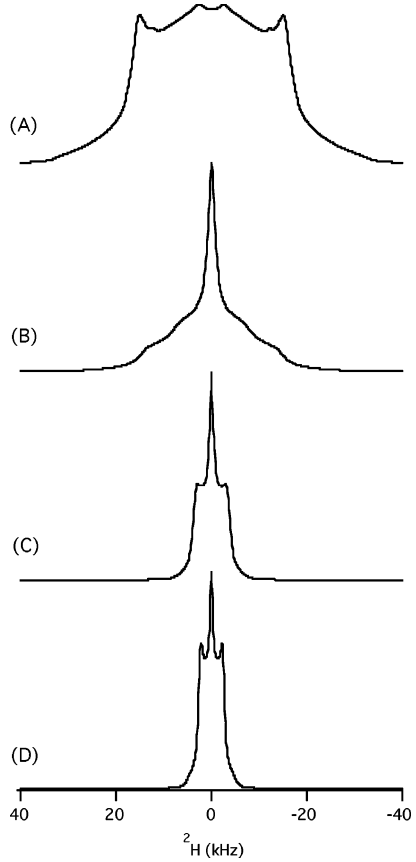

FIGURE 6: Simulations of CD_3-Leu NMR line shapes from the experimental ^{2}H NMR spectra displayed in Figure 3. Parameter inputs used in the MXQET program to create these model simulations are specified in the Materials and Methods and the Discussion. Simulations correspond to models for (A) all Leu-PLB spectra at −25 °C and Leu51 at 0 °C, (B) Leu28 and Leu39 at 0 °C and Leu51 at 25 °C, (C) Leu51 at 45 and 60 °C, and (D) Leu28 at 25, 45, and 60 °C.

The line shapes corresponding to CD_3-Leu51 (Figure 6A) indicate methyl site hopping motions with jump rates between 10 and 10^6 Hz and a superposition of a broad isotropic peak. The spectrum corresponding to CD_3-Leu at −25 °C is much broader than the other spectra collected at higher temperatures because of the slower side-chain motions at low temperatures. The ^{2}H quadrupolar splitting at −25 °C is consistent with previous studies that indicate that these residues are located inside the interior membrane, where the hydrocarbon chains are packed tightly in a crystalline lattice. Generally, for leucine residues in a crystalline lattice environment, the quadrupolar splitting is approximately 40 kHz (*34*, *44*). Therefore, the values recorded from these studies, provide evidence for the penetration of all three labeled leucines within the hydrophobic region of the bilayer, although such values are slightly smaller than 40 kHz. Because Leu51 is believed to be involved in helix−helix interactions (*13*), the resulting quadrupolar splitting is greater than that of the corresponding CD_3-Leu39 and CD_3-Leu28 spectra, which are more free to have other side-chain motions such as jumping between the predominant rotamers. This additional side-chain motion on the order of 10^2 Hz creates the more bell-shaped appearance of the Leu39 and Leu28 spectra at −25 °C as well as decreases the corresponding quadrupolar splittings by about 6 kHz (*34*). The broad isotropic peak in Figure 6A is attributed to residual water.

At 0 °C, the simulations of Leu28 and Leu39 in Figure 6B suggest that the ^{2}H NMR spectra contain three different components. The first component results from methyl group three-site jump rates of 1×10^7 Hz and two-site hopping motions with jump rates of 2×10^4 Hz; the second is a broader peak as in the lower temperature simulation; and the third is a sharp isotropic residual water peak. These two spectra are in stark contrast to the spectrum corresponding to Leu51 at 0 °C, which looks similar to the −25 °C spectra of Leu28 and Leu39 but with a sharp residual water isotropic peak in the center. This indicates that at 0 °C Leu51 is undergoing much slower methyl group motion with three-site rates equal to 1×10^6 Hz and two-site jumping rates on the order of 10^2 Hz.

At temperatures above 25 °C, the shape of the spectra of Leu39 (Figure 3B) is not easily simulated because of possible protein−lipid interactions. Molecular dynamic studies have indicated that fluctuations of both the lipids and the protein are much stronger at the hydrophobic core center of the lipid bilayer causing the side chain to be very mobile in that area (*62*, *63*). The ^{2}H NMR spectra of Leu39 are more complicated than the terminal amino acids because of the very different environments and different types of motions (such as librational) that are involved. At temperatures above 25 °C, Leu28 side chains undergo rapid motions associated with methyl group rotations as well as two-site hoping motions at jump rates corresponding to 1×10^8 and 6×10^8 Hz, respectively, as determined from the simulated spectrum, which also includes a sharp residual water isotropic component (Figure 6D).

^{2}H NMR spectra of Leu51 at 25, 45, and 60 °C provide the most unique information about TM-PLB in phospholipid bilayers. It is readily apparent that the quadrupolar splittings in the spectra are broader than both Leu39 and Leu28 at the same temperatures. This is the first indication of slower Leu51 side-chain motions, when compared to the other two residues. Also, the ^{2}H Leu51 NMR spectra (Figure 3) are more complicated. At 25 °C, the Leu51 spectrum has one component with similar features as the spectra of Leu28 and Leu39 at a lower temperature of 0 °C and a second component consisting of a Pake doublet with a splitting of about 8 kHz. We hypothesize that the unique side-chain motions observed in the Leu51 spectrum (at 25 °C) result from the superposition of two different oligomerization states of TM-PLB. This agrees with previous studies that indicated the coexistence of both pentameric and monomeric populations of full-length PLB (*16*, *58*, *59*). The fast moving less intense component (monomer) has rates comparable to Leu28 at 25 °C (Figure 6D), and a second slower dynamic component (pentamer) has rates similar to that of Figure 6B. Also, two components were not needed to simulate the Leu28 and Leu39 ^{2}H NMR spectra because they are not directly involved in the same Leu zipper formation as Leu51. At 45 °C, Leu51 can be simulated (Figure 6C) as a fast moving side chain with a strong isotropic peak in the center and three-site jump speeds of greater than 1×10^6 Hz and two-site jump rates of greater than 1×10^6 Hz. The Pake doublet is very similar to that of Leu28 except for a slightly larger quadrupolar splitting. The larger quadrupolar splitting indicates more restricted side-chain motion. The second population of TM-PLB in the monomeric form was taken under consideration in the 45 and 60 °C spectral simulations by modeling a fast moving side chain nearly identical to Leu28 and a superposition of a broader isotropic peak. The second component can be easily seen in the formation of the rounder bell-shape ^{2}H NMR spectrum of Leu51 at 60 °C.

Our results from the simulations agree well with previous studies on the PLB pentameric channel (*15*). Ying and co-workers have targeted Leu42, Leu43, and Leu44 in previous studies to establish the relative motion of the side chains and rotational reorientation of the phospholamban helices. The observed line shapes are identical with the line shapes from our ^{2}H NMR studies. The conclusions drawn from our studies agree with the mutagenesis studies by Adams and co-workers. Previous work by MacLennan and co-workers have proposed that Leu51 of full-length PLB is one of the residues lying on the interior face of the helix, stabilizing the pentamer (*64*). Thus, the slower Leu51 motion as simulated with the slower jump rates is probably due to restricted motion of this residue as a result of the side-chain orientation toward the helix interfaces that are involved in the leucine zipper motif.

Recent studies by Asahi and co-workers have observed enhanced physical interaction between SERCA1a and the Leu28 mutant, indicating that Leu28 is oriented toward the helix core (*65*). However, several studies have been carried out reporting contradictory results about the secondary structure of PLB in the membrane. One such model proposed that Leu28 lies in a position where it is a part of an antiparallel β-sheet region of the full-length PLB (*25*). Arkin and co-workers have argued on the basis of FTIR studies that the full-length PLB is α-helical (*24*). The partial ^{15}N backbone motional averaging of Leu28 (CSA of 170) indicates an α-helical peptide residue located toward the amino terminus and buried within the bilayer. As shown in Table 1, the magnitude of the difference between σ_{11} and σ_{33} corresponding to the breadth of the observed axially symmetric powder pattern is slightly different for all three residues within the limits of experimental error. The large breadth observed for Leu42 and Leu39 (CSA width of about 178 ppm) indicates that the carboxy-terminus residues of the peptide are relatively stable by virtue of backbone $i \rightarrow i + 4$ intramolecular hydrogen bonding (*38*). However, the ^{15}N CSA width of ^{15}N-labeled Leu28 is slightly reduced to 170 ppm, indicating the residue is weakly stabilized by backbone $i \rightarrow i + 4$ intramolecular hydrogen bonding when compared to Leu39 and Leu42 (*38*). It was also noted that, at −25 °C, the ^{15}N powder pattern spectrum of ^{15}N-labeled Leu28 has a slightly broader CSA (180 ppm) powder pattern when compared to the spectrum at 25 °C (data not shown). The difference in CSA width at the two temperatures is further evidence of increased mobility at the N terminus of the peptide at higher temperatures in the L_α phase. The ^{15}N CSA width of both ^{15}N-labeled Leu42 and Leu39 was 179 ppm at the two temperatures (−25 and 25 °C).

Chemical and molecular biological evidence supports the hypothesis that phospholamban exerts its action on Ca^{2+}-ATPase through direct protein−protein interactions (*21*). Hydrophobic interaction of the side chains accounts for the interactions of the two proteins. Evidence of such interactions was shown with a mutation on a zipper domain residue of I40LPLB (where isoleucine at position 40 was substituted with leucine), which was able to partially assemble into a pentamer yet decreased the apparent Ca^{2+} affinity of the

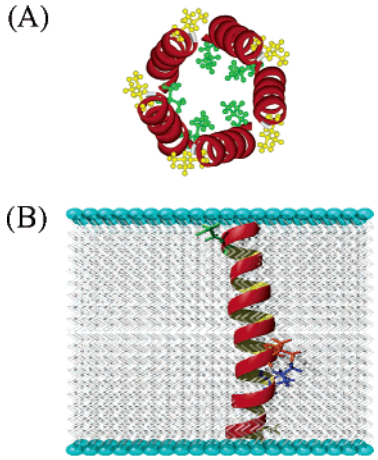

FIGURE 7: Structural models of TM-PLB in phospholipid bilayers showing the location of the leucine residues. (A) Pentamer model looking down the channel. Leu39, shown in yellow, is indicated as a surface residue and is not involved in helix−helix interactions. Leu51, shown in green, is involved in stabilizing the pentamer and is considered to be oriented inside the pentamer. (B) TM-PLB is displayed as a α-helical monomeric unit (for visual simplicity) showing the location of specific labeled residues within the bilayer.

pump as potently as a complete monomeric mutant substituted with Ala (*66*). Therefore, it is appropriate to assume that any residue within the zipper domain should have a potent effect on the Ca^{2+} pump and any residue adjacent to the pump has no effect on the pump. A model pentameric structure of full-length PLB was previously determined with a PDB code 1N7L and will be used to discuss our results (*67*). As shown in Figure 7A, the structure of the TM-PLB pentamer is composed of α-helical monomers, associated together through the interaction of specific residues. From our data, Leu51, which is shown in green, is among such residues involved in the helix−helix interaction inside the channel and is buried within the helix core, whereas Leu39 (shown in yellow) and Leu42 residues are pointing toward the lipid acyl chains and are not involved in helix−helix interactions (*23*). Therefore, the stabilization of the TM-PLB pentamer is due to the side chains of leucine and isoleucine of specific residues of the monomers interlocking in the crevices of opposite strands. The evidence of the type described above suggests that residues such as Leu51 within the zipper domain may be important regulatory components interacting with the pump, and a mutation of these residues will have a potent effect on the activity of the pump.

Structural Model of TM-PLB in Lipid Bilayers. Activity of a number of membrane proteins including the Ca^{2+}-ATPase has been shown to be dependent on bilayer thickness (*62*, *68*). The activity of the pump is highest when the ATPase is reconstituted into bilayers of di(18:1)PC, whereas the activity is lower in bilayers of shorter fatty acyl chains (*62*, *69*, *70*). The activity varies little in the chain-length range from C16 to C20, which is the range of fatty acyl chains found in the SR (*71*). The structural model displayed in Figure 7B for TM-PLB, indicates the location of the residues in POPC phospholipid bilayers. The hydrophobic thickness of POPC has been estimated to be about 27 Å. Assuming the number of amino acids per turn in an α-helix peptide is 3.6 residues and the pitch is 5.4 Å, then the translation per residue along the α-helical peptide will be 1.5 Å. Thus, to be able to span the hydrophobic region of the membrane, 18 residues are required, which places Leu39 near the center of the hydrophobic core of the POPC phospholipid bilayers. This agrees well with our ^2H NMR data of increased CD_3-Leu side-chain motion caused by acyl chains in the center of the bilayer. The phospholipid headgroups have a thickness of about 5 Å, which places Leu28 and Leu51 within the hydrophobic region of the lipids and very close to the polar headgroup toward the N- and C-terminal regions, respectively, of the TM-PLB peptide as depicted by the model in Figure 7B. This supports a TM-PLB segment that almost completely spans the bilayer and matches the bilayer thickness, thus having little to no tilt with respect to the bilayer.

CONCLUSION

In this paper, we have probed the dynamics of site-specific-labeled CD_3 groups of leucine in TM-PLB as a function of temperature. The quadrupolar splittings associated with the side-chain reorientations at lower temperatures were influenced by three-state jumps of the CD_3-Leu group. Upon increasing the temperature, $C_\alpha-C_\gamma$ and $C_\gamma-C_\delta$ rotations decreased the quadrupolar splittings. Leu51 spectra at all temperatures are slower moving than Leu28 and Leu39 spectra because of the involvement of Leu51 in the leucine zipper motif. Site-specific ^{15}N-labeled TM-PLB NMR studies were used to characterize the backbone dynamics, and our results indicated restricted motion for TM- PLB but subtle backbone mobility centered around Leu28. Finally, the 220-ppm ^{15}N chemical-shift value for ^{15}N-labeled Leu39 oriented in DOPC lipid bilayers indicates a helix that is nearly collinear with the bilayer normal. These results are displayed pictorially in the structural model of the monomer form of TM-PLB in the membrane (Figure 7B). The solid-state NMR data presented in this paper on TM-PLB does not specifically favor either of the two structural models (shown in Figure 1) for the full-length PLB pentamer. Future NMR experiments on the full-length PLB pentamer will address this issue.

REFERENCES

1. Li, H., Cocco, M. J., Steitz, T. A., and Engelman, D. M. (2001) Conversion of phospholamban into soluble pentameric helical bundle, *Biochemistry 40*, 6636−6645.
2. Fuji, J., Kadoma, M., Tada, H., and Sakiyama, F. (1986) Characterization of structural unit of phospholamban by amino acid sequencing and electrophoretic analysis, *Biochem. Biophys. Res. Commun. 138*, 1044−1050.
3. Kimura, Y., Kurzydlowski, K., Tada, M., and MacLennan, D. H. (1996) Phospholamban regulates the Ca^{2+}-ATPase through intramembrane interactions, *J. Biol. Chem. 249*, 6166−6173.
4. Cornea, R., Autry, J., Chen, Z., and Jones, L. (2000) Re-examination of the role of the leucine/isoleucine zipper residues of phospholamban in inhibition of the Ca^{2+}-pump of cardiac sarcoplasmic reticulum, *J. Biol. Chem. 275*, 41487−41494.
5. Minamisawa, S., Hoshijima, M., Chu, G., Martone, M. E., Wang, Y., Ross, J., Jr., Kranias, E. G., Giles, W. R., and Chien, K. R. (1999) Chronic phospholamban-sarcoplasmic reticulum calcium ATPase interaction is the critical calcium cycling defect in dilated cardiomyopathy, *Cell 99*, 313−322.
6. Simmerman, H. K., Collins, J. H., Theibert, J. L., Wegender, A. D., and Jones, L. R. (1996) Sequence analysis of phospholamban. Identification of phosphorylation sites and two major structural domains, *J. Biol. Chem. 261*, 13333−13341.
7. Young, H. S., Jones, L. R., Stakes, D. L. (2001) Location phospholamban in co-crystals with Ca^{2+}-ATPase by cryoelectron microscopy, *Biophys. J. 81*, 884−894.

8. Mascioni, A., Karim, C., Zamoon, J., Thomas, D. D., and Veglia, G. (2002) Solid-state NMR and rigid body molecular dynamics to determine domain orientations of monomeric phospholamban, *J. Am. Chem. Soc. 124*, 9392−9393.
9. Pollesello, P., Annila, A., and Ovaska, M. (1999) Structure of the 1−36 amino-terminal fragment of human phospholamban by nuclear magnetic resonance and modeling of the phospholamban pentamer, *Biophys. J. 76*, 1784−1795.
10. Lamberth, S., Schimidt, H., Muenchbach, M., Vorherr, T., Krebs, J., Carafoli, E., and Griesinger, C. (2000) NMR solution structure of phospholamban, *Helv. Chim. Acta 83*, 2141−2152.
11. Simmerman, H. K. B., Lovelace, D. E., and Jones, L. R. (1989) Secondary structure of detergent-solubilized phospholamban, a phosphorylatable, oligomeric protein of cardiac sarcoplasmic reticulum, *Biochim. Biophys. Acta*, 322−329.
12. Arkin, I. T., Adams, P. D., MacKenzie, K. R., Lemmon, M. A., Brunger, A. T., and Engelman, D. M. (1994) Structural organization of the pentameric transmembrane α helix of phospholamban, a cardiac ion channel, *EMBO J. 13*, 4757−4764.
13. Arkin, I. T., Adams, P. D., Aimoto, S., Engelman, D. M., and Smith, S. O. (1996) Structure of the transmembrane cysteine residues in phospholamban, *J. Membr. Biol.*
14. Birmachu, W., and Thomas, D. D. (1990) Rotational dynamics of the Ca-ATPase in sarcoplasmic reticulum studied by time-resolved phosphorescence anisotropy, *Biochemistry 29*, 3904−3914.
15. Smith, S. O., Kawakami, T., Liu, W., Ziliox, M., and Aimoto, S. (2001) Helical structure of phospholamban in membrane bilayers, *J. Mol. Biol. 313*, 1139−1148.
16. Cornea, R. L., Jones, L. R., Autry, J., and Thomas, D. D. (1997) Mutation and phosphorylation change the oligomeric structure of phospholamban in lipid bilayers, *Biochemistry 36*, 2960−2967.
17. Sasaki, T., Inui, M., Kimura, Y., Kuzuya, T., and Tada, M. (1992) Molecular mechanism of regulation of Ca^{2+} pump ATPase by phospholamban in cardiac sarcoplasmic-reticulum-effects of synthetic phospholamban peptides on Ca^{2+} pump ATPase, *J. Biol. Chem. 267*, 1674−1679.
18. Toyofuku, T., Kurzydlowski, K., Tada, M., and MacLennan, D. H. (1994) Amino acids GLU(2) to ILE(18) in the cytoplasmic domain of phospholamban are essential for functional association with the Ca^{2+}-ATPase of sarcoplasmic-reticulum, *J. Biol. Chem. 269*, 3088−3094.
19. Hughes, J., East, J. M., and Lee, A. G. (1994) The hydrophilic domain of phospholamban inhibits the Ca^{2+} transport step of the Ca^{2+}-ATPASE, *Biochem. J. 303*, 511−516.
20. Simmerman, H. K. B., Kobayashi, Y. M., Autry, J. M., and Jones, L. R. (1996) A leucine zipper stabilizes the pentameric membrane domain of phospholamban and forms a coiled-coil pore structure, *J. Biol. Chem. 271*, 5941−5946.
21. Adams, P. D., Arkin, I. T., Engelman, D. M., and Brunger, A. T. (1995) Computational searching and mutagenesis suggest a structure for the pentameric transmembrane domain of phospholamban, *Nat. Struct. Biol. 2*, 154−162.
22. Ahmed, Z., Reid, D. G., Watts, A., and Middleton, D. A. (2000) A solid-state NMR study of the phospholamban transmembrane domain: Local structure and interactions with Ca^{2+}-ATPase, *Biochim. Biophys. Acta 1468*, 187−198.
23. Hughes, E., and Middleton, D. A. (2003) Solid-state NMR reveals structural changes in phospholamban acompanying the functional regulation of Ca^{2+}-ATPase, *J. Biol. Chem. 278*, 20835−20842.
24. Arkin, I. T., Rothman, M., Ludlam, C. F., Aimoto, S., Engelman, D. M., Rothschild, K. J., and Smith, S. O. (1995) Structural model of the phospholamban ion channel complex in phospholipid membranes, *J. Mol. Biol. 248*, 824−834.
25. Tatulian, S. A., Jones, L. R., Reddy, L. G., Stokes, D. L., and Tamm, L. K. (1995) Secondary structure and orientation of phospholamban reconstituted in supported bilayers from polarized attenuated total reflection FTIR spectroscopy, *Biochemistry 34*, 4448−4456.
26. Frank, S., Kammerer, R. A., Hellstern, S., Pegoraro, S., Stefeld, J., Lustig, A., Moroder, L., and Engel, J. (2003) Toward a high-resolution structure of phospholamban: Design of soluble transmembrane domain mutants, *Biochemistry 39*, 6825−6831.
27. Prosser, R. S., Daleman, S. I., and Davis, J. H. (1994) The structure of an integral membrane peptide: A deuterium NMR study of gramicidin, *Biophys. J. 66*, 1415−1428.
28. Sharpe, S., Barber, K. R., and Grant, W. M. (2002) Evidence of a tendency to self-association of the transmembrane domain of ErbB-2 in fluid phospholipid bilayers, *Biochemistry 41*, 2341−2352.
29. Koenig, B. W., Ferreti, J. A., and Gawrisch, K. (1999) Site-specific deuterium order parameters and membrane-bound behavior of a peptide fragment from the intracellular domain of HIV-1 gp41, *Biochemistry 38*, 6327−6334.
30. Mack, J. W., Torchia, D. A., and Steinert, P. M. (1988) Solid-state NMR studies of the dynamics and structure of mouse keratin intermediate filaments, *Biochemistry 27*, 5418−5426.
31. Beshah, K., Olejniczak, E. T., and Griffin, R. G. (1987) Deuteriun NMR study of methyl group dynamics in L-alanine, *J. Chem. Phys. 86*, 4730−4736.
32. Keniry, M. A., Kintanar, A., Smith, R. L., Gutowsky, H. S., and Oldfield, E. (1984) Nuclear magnetic resonance of amino acids and proteins. Deuterium nuclear magnetic resonance relaxation of deuteriomethyl-labeled amino acids in crystals and in halobacterium halobium and *E. coli* cell membranes, *Biochemistry 23*, 288−298.
33. Batchelder, L. S., Sullivan, C. E., Jelinski, L. W., and Torchia, D. A. (1982) Characterization of leucine side-chain reorientation in collagen-fibrils by solid-state deuterium NMR, *Proc. Natl. Acad. Sci. U.S.A. 79*, 386-389.
34. Ying, W., Irvine, S. E., Beekman, R. A., Siminovitch, D. J., and Smith, S. O. (2000) Deuterium NMR reveals helix packing interactions in phospholamban, *J. Am. Chem. Soc. 122*, 11125−11128.
35. Kinsey, R. A., Kintanar, A., and Oldfield, E. (1981) Dynamics of amino acid side chains in membrane proteins by high field solid-state deuterium nuclear magnetic resonance spectroscopy, *J. Biol. Chem. 256*, 9028−9036.
36. Leo, G. C., Colnago, L. A., Valentine, K. G., and Opella, S. J. (1987) Dynamics of fd coat protein in lipid bilayers, *Biochemistry 26*, 854−862.
37. Whiles, J. A., Brasseur, R., Glover, K. J., Melacini, G., Komives, E. A., and Vold, R. R. (2001) Orientation and effects of mastoparan X on phospholipid bicelles, *Biophys. J. 80*, 280−293.
38. Jones, D. H., Rigby, A. C., Barber, K. R., and Grant, W. M. (1997) Oligomerization of the EGF receptor transmembrane domain: A ^{2}H NMR study in lipid bilayers, *Biochemistry 36*, 12616−12624.
39. Van der Wel, P. C. A., Strandberg, E., Killian, J. A., and Koeppe, R. E., II (2002) Geometry and intrinsic tilt of a tryptophan-anchored transmembrane α-helix determined by deuterium NMR, *Biophys. J. 83*, 1479−1488.
40. Killian, J. A., Taylor, M. J., and Koeppe, R. E., II (1992) Orientation of the valine-1 side chain of the gramicidin transmembrane channel and implications for channel functioning: A deuterium NMR study, *Biochemistry 31*, 11283−11290.
41. Lee, K.-C., Huo, S., and Cross, T. A. (1995) Lipid-peptide interface: Valine conformation and dynamics in the gramicidin channel in a lipid bilayer, *Biochemistry 34*, 857−867.
42. Janin, J., and Wodak, S. (1978) Conformation of amino acid side-chain in proteins, *J. Mol. Biol. 125*, 357−386.
43. Keniry, M. A. (1989) Solid-state deuterium nuclear magnetic resonance spectroscopy of proteins, *Methods Enzymol. 176*, 376−386.
44. Batchelder, L. S., Sullivan, C. E., Jelinski, L. W., and Torchia, D. A. (1982) Characterization of leucine side-chain reorientation in collagen-fibrils by solid-state ^{2}H NMR, *Proc. Natl. Acad. Sci. U.S.A. 79*, 386-389.
45. Lee, K.-C., and Cross, T. A. (1994) Side-chain structure and dynamics at the lipid−protein interface: Val1 of the gramicidin A channel, *Biophys. J. 66*, 1380−1387.
46. Tiburu, E. K., Dave, P. C., Vanlerberghe, J. F., Cardon, T. B., Minto, R. E., and Lorigan, G. A. (2003) An improved synthetic and purification procedure for the hydrophobic segment of the transmembrane peptide phospholamban, *Anal. Biochem. 318*, 146−151.
47. Davis, J. H., Jeffrey, K. R., Bloom, M., and Valic, M. I. (1976) Quadrupolar echo deuterium magnetic resonance spectroscopy in ordered hydrocarbon chains, *Chem. Phys. Lett. 42*, 390−394.
48. Pines A., Gibby, M., and Waugh, J. S. (1973) Proton-enhanced NMR of dilute spins in solids, *J. Chem. Phys. 59*, 569−590.
49. Massiot, D., Fayon, F., Capron, M., King, I., Le Calve, S., Alonso, B., Durand, J. O., Bujoli, B., Gan, Z., and Hoatson, G. (2002) Modeling one- and two-dimensional solid-state spectra, *Magn. Reson. Chem. 40*, 70−76.

50. Greenfield, M. S., Ronemus, A. D., Vold, R. L., Vold, R. R., Ellis, P. D., and Raidy, T. E. (1987) Deuterium quadrupole-echo NMR spectroscopy III. Practical aspects of line shape calculations for multiaxis rotational processes, *J. Magn. Reson. 72*, 89−107.
51. Wildman, K. A. H., Lee, K.-D., and Ramamoorthy, A. (2003) Mechanism of lipid bilayer disruption by the human antimicrobial peptide, LL-37, *Biochemistry 42*, 6545−6558.
52. Hartzell, C. J., Whitfiled, M., Oas, T. G., and Drobny, G. P. (1987) Determination of the ^{15}N and ^{13}C chemical shift tensors of L-[^{13}C]-alany-L-[^{15}N]alanine from the dipole-coupled powder patterns, *J. Am. Chem. Soc. 109*, 5966−5969.
53. Ketchem, R. R., Hu, W., and Cross, T. A. (1993) High-resolution conformation of gramicidin-A in a lipidbilayer by solid-state NMR, *Science 261*, 1457−1460.
54. Keniry, M. A., Gutowsky, H. S., and Oldfield, E. (1984) Surface dynamics of the integral membrane-protein bacteriorhodopsin, *Nature 307*, 383−386.
55. Opella, S. J., Frey, M. H., and Cross, T. A. (1979) *J. Am. Chem. Soc. 101*, 5856−5857.
56. Ulrich, A. S., Watts, A., Wallat, I., and Heyn, M. P. (1994) Distorted structure of retinal chromophore in bacteriorhodopsin resolved by deuterium NMR, *Biochemistry 33*, 5370−5375.
57. Prosser, R. S., and Davis, J. H. (1994) Dynamics of an integral membrane peptide: A deuterium NMR relaxation study of gramicidin, *Biophys. J. 66*, 1429−1140.
58. Reddy, L. G., Jones, L. R., and Thomas, D. D. (1999) Depolymerization of phospholamban in the presence of calcium pump: A fluorescence energy transfer study, *Biochemistry 38*, 3954−3962.
59. Li, M., Reddy, L. G., Bennett, R., Silva, N. D., Jr., Jones, L. R., and Thomas, D. D. (1999) A fluorescence energy transfer method for anlayzing protein oligomeric structure: Application to phospholamban, *Biophys. J. 76*, 2587−2599.
60. Lovell, S. C., Worde, J. M., Richardson, J. S., and Richardson, D. C. (2000) The penultimate rotamer library, *Proteins 40*, 389−408.
61. Wittebort, R. J., Olejniczak, E. T., and Griffin, R. G. (1987) Analysis of deuterium nuclear magnetic resonance line shapes in anisotropic media, *J. Chem. Phys. 86*, 5411−5420.
62. Lee, A. G. (2003) Lipid−protein interactions in biological membranes: A structural perspective, *Biochim. Biophys. Acta 1612*, 1−40.
63. Berendsen, H. J. C., and Tieleman, D. P. (1998) Lipid−protein systems: History and methods, *Bichim. Biophys. Acta 3*, 1639−1650.
64. Johnson, R. G., and Kranias, E. (1823−1998) Cardiac sarcoplasmic reticulum function and regulation of contractility, *Ann. N.Y. Acad. Sci. 853*, 31−42.
65. Asahi, M., Green, N. M., Kurzydlowski, K., Tada, M., and MacLennan, D. H. (2001) Phospholamban domain IB forms an interaction site with the loop between transmembrane helices M6 and M7 of sarco(endo)plasmic reticulum Ca^{2+} ATPases, *Proc. Natl. Acad. Sci. U.S.A. 98*, 10061−10066.
66. Simmerman, H. K., Kobayashi, Y. M., Autry, J. M., and Jones, D. H. (1996) A leucine zipper stabilizes the pentameric membrane domain of phospholamban and forms a coiled-coil pore structure, *J. Biol. Chem. 270*, 5941−5946.
67. Zamoon, J., Macioni, A., Thomas, D. D., and Veglia, G. (2003) *Biophys. J. 85*, 2589.
68. Johannsson, A., Smith, G. A., and Metcalfe, J. C. (1981) The effects of bilayer thickness on the activity of (Na/K)-ATPase, *Biochim. Biophys. Acta 641*, 416−421.
69. Johannsson, C. A., Keightley, G. A., Smith, C. D., Richards, T. R., Hesketh, J. C., and Metcalfe, J. C. (1981) The effect of bilayer thickness and normal-alkanes on the activity of the (Ca/Mg)-dependent ATPase of sarcosplasmic reticulum, *J. Biol. Chem. 256*, 1643−1650.
70. Starling, J. P., East, J. M., and Lee, A. G. (1996) Separate effects of long-chain phosphatidylcholines on dephosphorylation of the Ca^{2+}-ATPase and on Ca^{2+} binding, *Biochem. J. 318*, 785−788.
71. Gould, G. W., McWhirter, J. M., East, J. M., and Lee, A. G. (1987) Uptake of Ca^{2+} mediated by the (Ca/Mg)-ATPase in reconstituted vesicles, *Biochem. J. 245*, 751−755.

BI0490993